

# A 14.5 $\mu\text{V}_{\text{rms}}$ 2.55 $\mu\text{W}$ Fully Integrated CMOS Preamplifier for Non-Invasive Wearable Electrocardiogram Sensor Applications

Krishna Gupta<sup>1</sup> and Shivaji Tyagi<sup>1</sup>

<sup>1</sup>Jaypee Institute of Information Technology

June 6, 2023

## Abstract

In this paper, a noise and power-optimized fully-differential capacitive feedback CMOS preamplifier circuit is designed using a commercial 0.35  $\mu\text{m}$  CMOS technology node. The designed preamplifier circuit is part of an analog front-end SoC, which monitors the human electrocardiogram (ECG) using dry electrodes. The transistors in the interface circuit are biased in weak inversion region for lower total input referred noise and power dissipation respectively. With an input referred noise of 14.5  $\mu\text{V RMS}$  and 2.55  $\mu\text{W}$  power dissipation, the resultant preamplifier achieves a gain of 52dB over a bandwidth range of 0.003 Hz to 880 Hz with Noise Efficiency Factor (NEF) of 2.52.

## ARTICLE TYPE

# A $14.5 \mu V_{rms}$ $2.55 \mu W$ Fully Integrated CMOS Preamplifier for Non-Invasive Wearable Electrocardiogram Sensor Applications

Krishna Gupta\* | Shivaji Tyagi

<sup>1</sup>Department of Electronics and Communication Engineering, Jaypee Institute of Information Technology, Uttar Pradesh, India

**Correspondence**

\*Krishna Gupta, Jaypee Institute of Information Technology, Sector 62, Noida. Email: krishna.gupta21100@gmail.com

**Abstract**

In this paper, a noise and power-optimized fully-differential capacitive feedback CMOS preamplifier circuit is designed using a commercial  $0.35 \mu m$  CMOS technology node. The designed preamplifier circuit is part of an analog front-end SoC, which monitors the human electrocardiogram (ECG) using dry electrodes. The transistors in the interface circuit are biased in weak inversion region for lower total input referred noise and power dissipation respectively. With an input referred noise of  $14.5 \mu V_{RMS}$  and  $2.55 \mu W$  power dissipation, the resultant preamplifier achieves a gain of 52dB over a bandwidth range of 0.003 Hz to 880 Hz with Noise Efficiency Factor (NEF) of 2.52.

**KEYWORDS:**

electrocardiogram; low-noise; low-power; dry-electrode; CMRR

## 1 | INTRODUCTION

With advancements in technology, there has been a rise in the usage of portable, low-power biomedical equipment in clinics and hospitals over the past few years. This is especially true for electrocardiogram (ECG) measurement tools since increasing research has shown that ECG is a precise way to measure heart rate in the realms of medicine, sports, and athletics. Furthermore, patients with chronic conditions and a higher risk of heart attack require regular monitoring, which enhances the need for the design of lightweight, cost-effective, and low-power consumption monitoring equipment.

Biomedical signals have low voltage and low frequency, making recording tedious. Peak voltages for the majority of biological signals, such as the ECG and EEG, range from  $10 \mu V$  to  $100 mV$ , while frequencies range from  $0.1 Hz$  to  $500 Hz$ . The amplitude and frequency spectra of a few biological signals are shown in Figure 1. Additionally, due to their inherent characteristics, common mode noise's amplitude may be higher than the actual signal's amplitude. As a result, a high Common Mode Rejection Ratio (CMRR) is necessary to amplify weak biological signals appropriately and reject unwanted noise.

### 1.1 | ECG Characteristics

The voltage produced by the cardiac or heart muscle during a heartbeat is explicitly traced on an electrocardiogram or ECG. It gives a highly precise assessment of how well the heart is working. A pacemaker, which starts the cardiac cycle by receiving electrical impulses from the neurological system, regulates the heart's beating. A unique form of cell called a myocyte, which has the mechano-chemical ability to physically contract upon activation, is found in the heart muscles. The cell may be seen as a network of channels that carry different ions, including potassium, sodium, calcium, and chlorine.<sup>1</sup>

<sup>0</sup>Abbreviations: CMRR, Common Mode Rejection Ratio; ECG, Electrocardiogram; NEF, noise efficiency factor

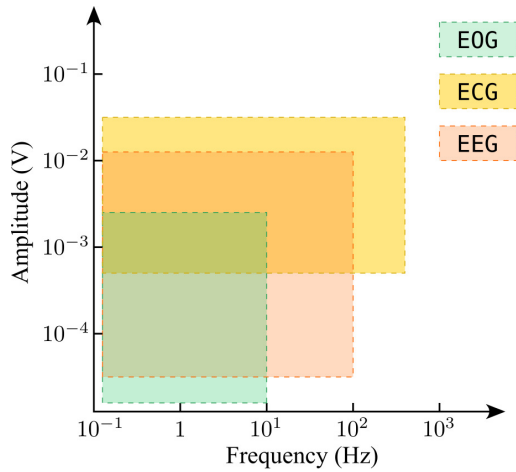


FIGURE 1 Frequency Spectra of Biomedical Signals

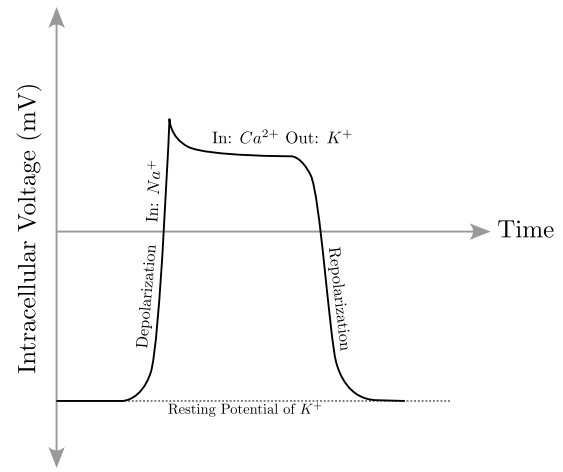


FIGURE 2 Intra-cellular Potential during Excitation

The potassium channel has a substantially lower resistance at rest than other channels; hence, the potassium Nernst potential, or roughly -90 mV, is the cell's resting potential. The sodium channel's resistance rapidly reduces to a level that is 100–1000 times lower than the potassium channel's resistance upon stimulation, causing the cellular potential to increase to the sodium's Nernst potential or roughly +40 mV. This is shown in Figure 2. "Depolarization" is the term used to describe this phenomenon.

Following this, calcium begins to enter the cell, causing the cellular potential to stabilize for a brief time at a steady voltage. The cell begins to contract at this particular moment. After this, potassium begins to enter the cell once more, and the cell regains its resting potential, a process known as "re-polarization." Figure 2 depicts the relationship between cell potential and time.

All of this takes place starting with the sino-atrial (SA) node, where the atrium's surrounding muscles contract first, and moving down to the atrioventricular (AV) node, where the ventricle's muscles contract. The ECG seen in figure 3 is the result of the vector summation of the cell potential at various nodes that make up the cardiac muscles.

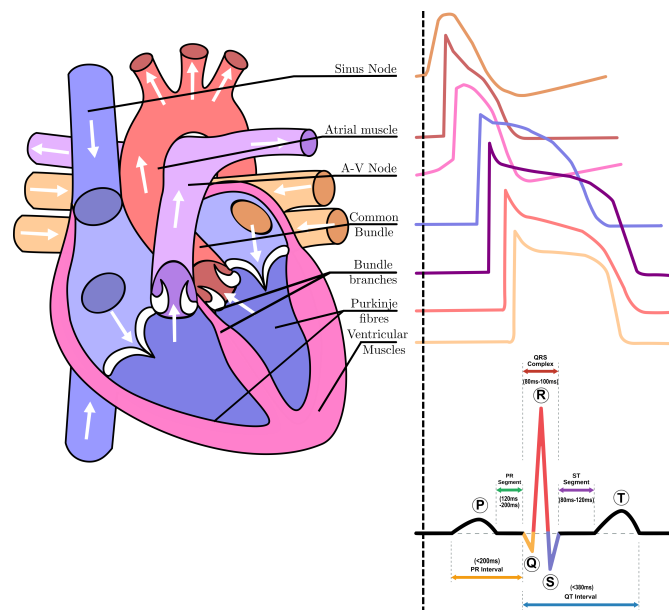


FIGURE 3 Formation of ECG Wave: Atrial activation results in the P wave, ventricular depolarization causes the QRS complex, and ventricular repolarization causes the T wave.<sup>2</sup>

We can monitor these signals by putting electrodes on the skin's surface since all of these phenomena are electrical and might easily conduct in the body, which is full of fluids. The sole downside is that no equipment can directly pick up these signals due to their extremely low amplitude and the risk of picking up extraneous signals. Therefore, we must create a system to filter the unwanted noise while also enhancing these weak biological signals with the proper amount of gain.

## 2 | DESIGN REQUIREMENTS

### 2.1 | Skin Electrode Interface

Chronic patients, such as those with an increased risk of myocardial infarction, require portable electro-physiological monitoring technology, such as miniature cardiac tags. The signal-degrading effects of the electrodes during extended application times justify the selection of electrodes. We only have a few electrode options because this work primarily focuses on non-invasive monitoring: dry and wet electrodes. Wet electrodes are similar to dry electrodes, but they also include a solution of silver chloride to lower contact impedance and lower motion artifacts. The disadvantage of utilizing wet electrodes is that AgCl dries out with time, increasing the electrode's contact impedance, which raises the offset voltage that the electrode induces.

Because the electrodes will be worn for extended periods, the silver chloride may also irritate the skin and, in rare instances, lead to cyanosis<sup>3</sup>. For longer-term electrophysiological signal monitoring, dry electrodes are the preferred option. Adding more contact sites between the skin and the skin-electrode interface might reduce the contact impedance. A pre-amplifier and, subsequently, competent software might be used to neutralize the extra noise the system creates by digital means.

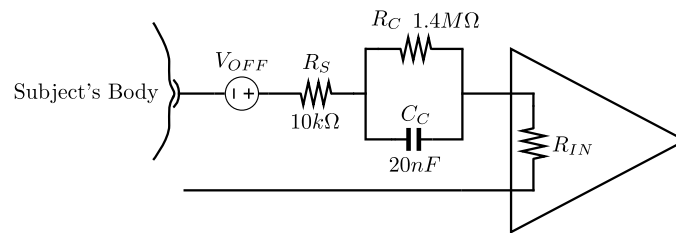


FIGURE 4 Dry Electrode Skin Interface Model

To create electrical models for electrodes, several sophisticated research has been carried out<sup>4,5</sup>. Figure 4, which is the model the authors mostly employ, is straightforward yet effective. The offset voltage caused by the electrode is represented by  $V_{OFF}$ .  $R_C$  and  $C_C$  indicate the coupling impedance of the electrode to the body, while  $R_S$  stands for series resistance.

### 2.2 | Input Impedance Requirements

According to AAMI, we require a signal-to-interference ratio better than 40 dB for diagnostic ECG sensing. We can disregard the coupling impedance depicted in figure 4 if there is perfect contact between the electrode and skin. As a result,  $R_S$  might be used to indicate the electrode's overall resistance. An additional electrode with series resistance  $R_s$  will be in the lead-II ECG. Each of these may be represented by  $R_{S1}$  and  $R_{S2}$  respectively. Using  $R_{IN}$  as the amplifier's input impedance, the identical differential signal, represented as  $V_{id}$  with common mode as  $V_{CM}$ , is applied at the inputs. We can write:

$$V_{id,1} - V_{id,2} = V_{id} \left(1 - \frac{R_{S1} - R_{S2}}{2R_{IN}}\right) + V_{CM} \left(\frac{R_{S2} - R_{S1}}{R_{IN}}\right) \quad (1)$$

Equation 1 shows that the output signal may contain parts of the common mode noise, which is occurring due to a mismatch in electrode resistances. Assuming 40 dB SNR (or signal-to-interference ratio), the ratio of differential to common mode signal components must be larger than 40 dB, which corresponds to:

$$R_{IN} > 100 \frac{V_{CM}}{V_{id}} (R_{S2} - R_{S1}) \quad (2)$$



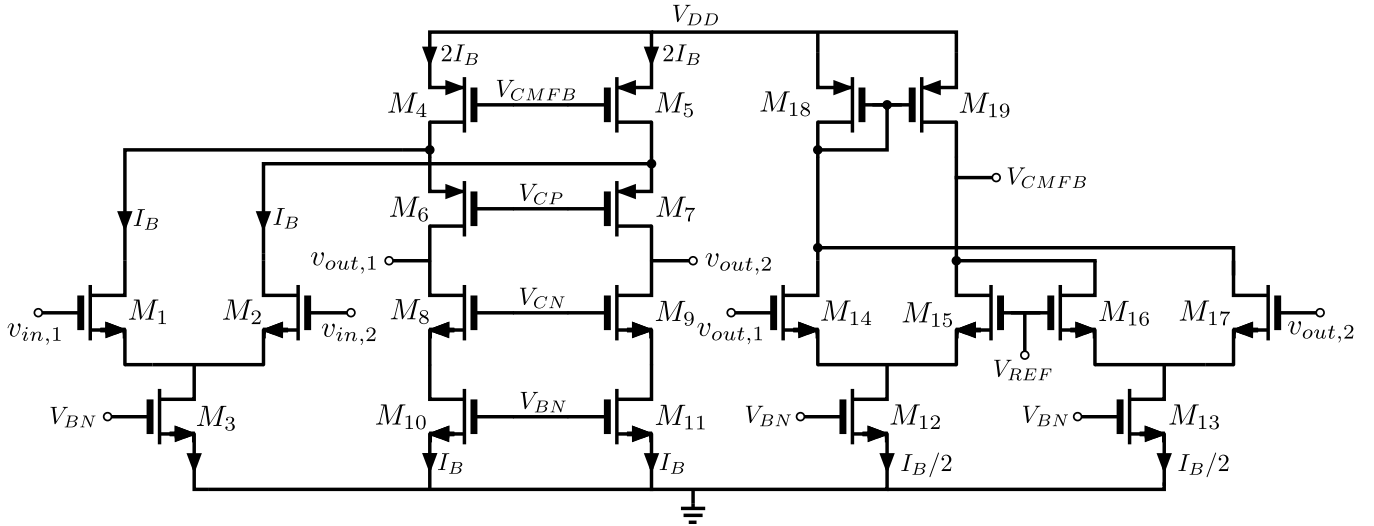


FIGURE 7 Fully Differential Folded Cascode OTA

The mid-band gain is determined by the proportion of  $C_1$  to  $C_2$ . The approximate bandwidth of the circuit is given by  $g_m/A_{mid}C_L$ , where  $g_m$  denotes the transconductance of the operational transconductance amplifier.

### 3.1 | Design of Pseudo Resistors

Each PMOS device operates as a diode-connected MOS transistor with negative  $V_{GS}$ . Positive  $V_{GS}$  activates the parasitic p-n-p bipolar junction transistor (BJT), which then performs like a diode-connected BJT. As seen in figure 6, the resistance is quite high for very few voltage fluctuations across this device. The tera-ohm range corresponds to the resistance measured throughout a 0.1-0.2 V voltage fluctuation. The resistance dip occurs at 0 V potential difference across it.  $1/2\pi R_{in}C_2$  handles the lower frequency cutoff. The resistance starts to quickly drop when there is a big enough voltage differential between them. Large value resistors have been obtained in amplifier designs by biasing transistors in the sub-threshold region; however, this requires extra bias circuitry, which increases power consumption.

### 3.2 | Design of Low-noise Operational Transconductance Amplifier

The proposed low-noise ECG preamplifier uses a fully differential folded cascode OTA scheme as shown in Figure 7. The constant transconductance bias circuit is used to bias the gates of  $M_4$  to  $M_{11}$ . Standard fully differential folding cascode circuit architecture is employed, which performs better than single-ended topology due to an improved common mode rejection ratio, which is a crucial aspect of ECG amplifier design. The transistors must be sized at the proper inversion levels to minimize noise and power consumption. The reference voltage  $V_{REF}$  is generated using a bandgap reference circuit to make the design invariant to temperature and voltage fluctuations<sup>8</sup>.

According to [Young (2019)]<sup>9</sup>, we require a gain of at least 40 dB over a bandwidth of 800 Hz to 1 kHz to meet ECG criteria. In light of this, we determine that our bias current,  $I_B$ , is 100 nA. Depending on the W/L ratio, each transistor functions in weak or moderate inversion at this bias current.

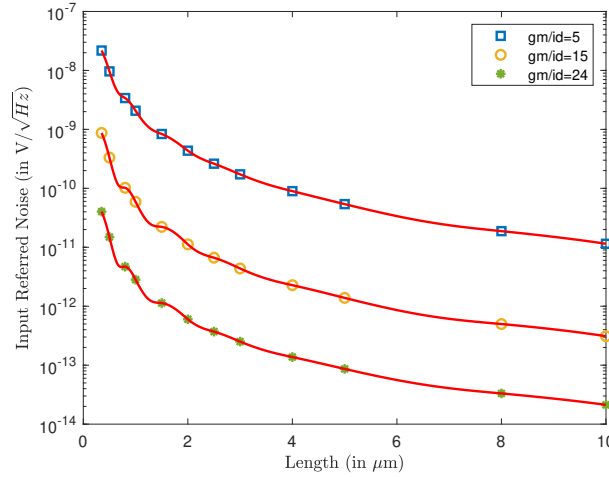
We determine the device's current efficiency to scale the transistors using:

$$\frac{g_m}{I_D} = \frac{2}{V_{OV}} \quad (6)$$

$V_{OV}$  stands for the device's overdrive voltage, which also describes the degree of channel inversion<sup>10</sup>. A device that runs in strong inversion and has  $g_m/id < 10$  has a higher  $V_{OV}$ . Similar to this, devices that function in moderate inversion ( $g_m/id$  between 10 and 20) and weak inversion ( $g_m/id > 20$ ) have lower overdrive voltages. For all the devices shown in figure 7, Table 1 displays the drain currents and operational parameters.

**TABLE 1** Device Parameters of Folded-Cascode Closed-Loop ECG Preamplifier

Devices	$I_D(nA)$	$gm/id(V^{-1})$	$V_{ov}$
$M_1, M_2$	136.9	23.06	46 mV
$M_4, M_5$	192.3	23.09	54 mv
$M_6, M_7, M_8, M_9$	106.54	23.96	53 mV
$M_{10}, M_{11}$	106.2	21.95	45 mV

**FIGURE 8** Input Referred Noise vs L

Our input pair has to be biased into weak inversion for low power usage and noise reduction. In a weak inversion, the drain current is provided by:

$$I = \mu C_{OX} \left(\frac{1}{m}\right) \left(\frac{W}{L}\right) \left(\frac{n_1 kT}{q}\right)^2 \exp\left[\frac{q}{n_1 kT} \left(V_{GS} - V_{TH} - \frac{n_1 kT}{q}\right)\right] \left[1 - \exp\left(\frac{-mqV_{DS}}{n_1 kT}\right)\right] \quad (7)$$

where  $k$  denotes Boltzmann constant,  $T$  is the temperature,  $q$  denotes the electron charge, and  $W$  and  $L$  are the transistor's dimensions;  $\mu$  is the effective mobility; and  $C_{OX}$  is an oxide capacitance.  $m$  and  $n_1$  are the process parameters.

As ECG is a low-frequency signal, flicker noise is more dominant, thereby a perfect choice for optimization. The flicker noise of a MOS transistor is given by:

$$\overline{V_{in,fn}^2} = \frac{K_f}{C_{OX} W L} \frac{1}{f} \quad (8)$$

As we can see, expanding the area of devices is necessary to lessen flicker noise. By biasing the devices into weak inversion, this might be accomplished. Weak inversion is a good option to lower the overall noise of the circuit since better current efficiency values result in a lower noise response as shown in figure 8. The graph was produced using the device characterization data from the 0.35um technology node.

The common mode feedback circuit, shown in figure 7 by  $M_{12} - M_{19}$  is a continuous time differential feedback circuit. The reference voltage ( $V_{REF}$ ) is produced using a bandgap reference circuit for independence over temperature variations. Using the split-MOS technique the voltage  $V_{CMFB}$  is applied to the gates of  $M_4$  and  $M_5$ . The CMFB circuit has no impact on input referred noise because it is only used to set the output common mode level.

The noise efficiency factor (NEF) proposed in [Najafi and Wise (1986)]<sup>11</sup> may be calculated since we want to minimize both power and noise. NEF is given by:

$$NEF = \sqrt{\frac{4I_{tot}}{3U_T g_{m1-2}}} \quad (9)$$

$I_{tot}$  for the design is 382.6 nA, substituting the required parameters in equation 9 we get:

$$NEF = \sqrt{\frac{4 \times 382.6nA}{3 \times 25.6mV \times 3.136\mu}} \approx 2.52 \quad (10)$$

## 4 | SIMULATION RESULTS

The amplifier is designed Using Mentor Graphics Pyxis Design Environment using a commercial 0.35um CMOS process. The novel architecture simulation results for a capacitive load of 1 pF and single supply of 3.3 V achieves a gain of 52 dB spanning a bandwidth of 0.003 Hz to 880 Hz, when  $C_1$  and  $C_2$  were set to 100u and 100p, respectively. This is seen in the AC Response in figure 9 . The large bandwidth is necessary for proper reading of the QRS complex as insufficient bandwidth results in rounding-off of the sharp ECG characteristics and reduction in strength of the QRS complex<sup>12</sup>. Table 2 shows simulated outcomes for different design parameters as well as a comparison with current industry standard designs.

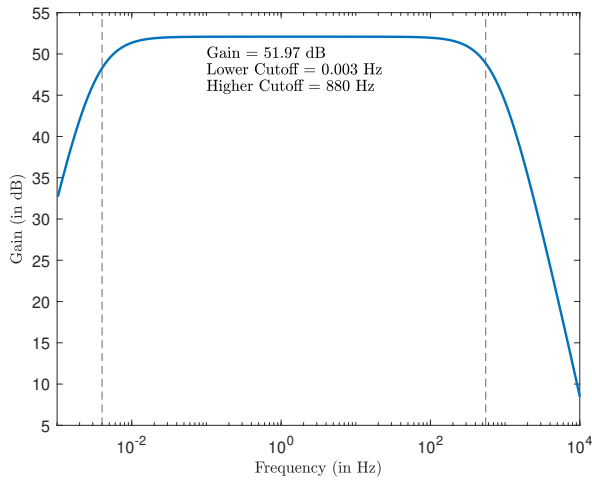


**FIGURE 9** AC Response of ECG Amplifier

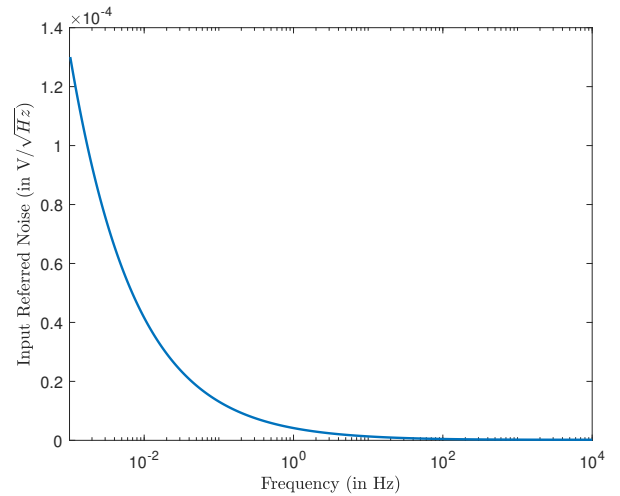


**FIGURE 10** Noise Response of ECG Amplifier

The noise analysis of the proposed circuit is shown in Figure 10 . We obtain the RMS noise voltage by integrating across the specified bandwidth which is calculated to be  $14.5\mu V_{RMS}$ . The input-referred noise is higher due to the increased bandwidth requirements of an ECG<sup>12</sup>. Due to the circuit's small bandwidth and the requirement that input-referred noise only is lower than the usual extracellular neuronal background noise of  $5-10 V_{RMS}$  over this bandwidth<sup>13</sup>, this noise level is acceptable.

The results of a process variation study across gain, unity gain frequency, lower-3dB, and upper-3dB cutoff frequencies were 1% to 8% relative standard deviation, which is significantly less than the permitted maximum variation. Over 100 samples were analyzed.

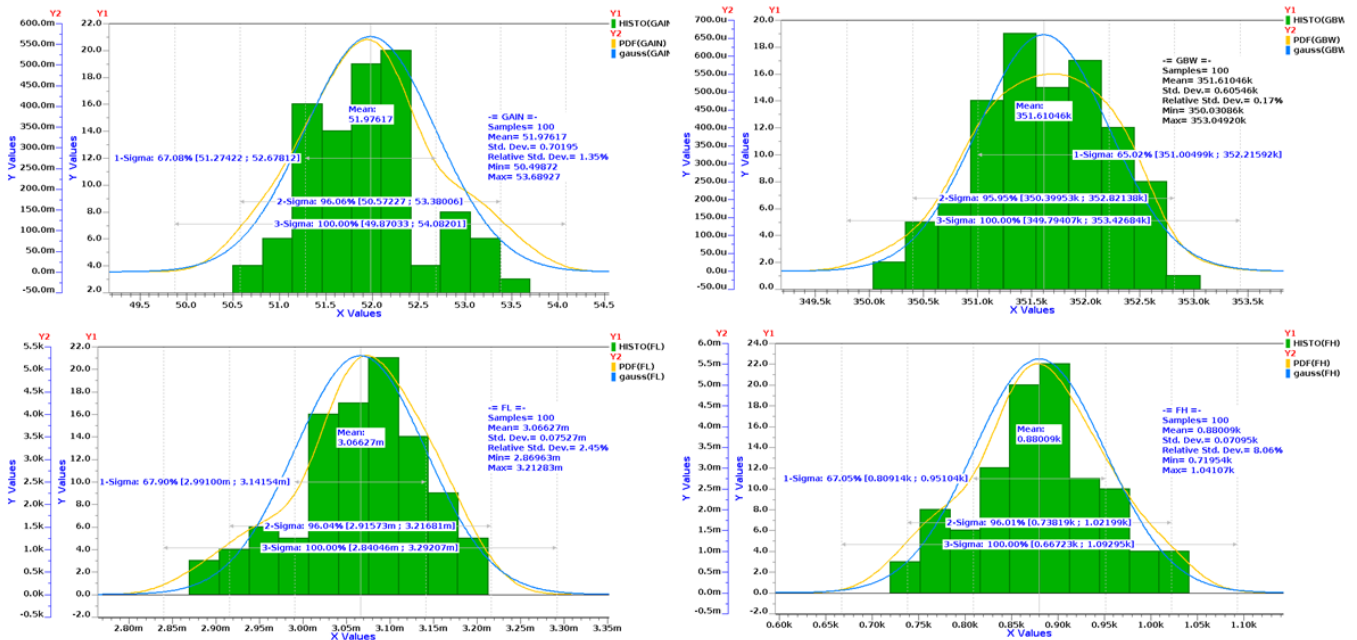
Process variation corresponds to various manufacturing defects and non-perfections such as variation in diffusion resistances due to doping, or irregular thickness of oxide on top of silicon substrate. This causes variations in parameters such as mobility, threshold voltage, etc. Our design surpasses such variations as the sensitivity corresponding to the mean per standard deviation is below 8% for all parameters. Other factors such as supply voltage and temperature variation were simulated and the major variation factor was pseudo resistors but under all Process, Voltage, and Temperature variations, our designs showed 1.35%

**TABLE 2** Comparative Analysis of ECG Amplifier

Parameter	[Harrison and Charles] <sup>7</sup>	[Fay et al.] <sup>1</sup>	[Zhnag et al.] <sup>14</sup>	[Saeidian et al.] <sup>15</sup>	This Work
Supply Voltage	$\pm 2.5$	3	2	1	3.3
Total Current	16 $\mu\text{A}$	1.08 $\mu\text{A}$	160 nA	71.2nA	770 nA
Gain	40 dB	45.3 dB	39.8 dB	55 dB	52 dB
Bandwidth	7.5 kHz	290 Hz	200 Hz	263.6 Hz	880 Hz
Low Cut-off Frequency	0.130 Hz	NA	0.2 Hz	0.37 Hz	0.003 Hz
Input Referred Noise	2.1 $\mu\text{Vrms}$	8.1 $\mu\text{Vrms}$	2.05 $\mu\text{Vrms}$	9.6 $\mu\text{Vrms}$	14.5 $\mu\text{Vrms}$
NEF	3.8	NA	2.26	6.1	2.52
CMRR	> 42 dB	90 dB (at 60 Hz)	> 70 dB	81.5 dB	> 80 dB
PSRR	> 42 dB	NA	> 65 dB	53 dB	> 80 dB
Power Consumption	80 $\mu\text{W}$	2.76 $\mu\text{W}$	560 nW	71.2nW	2.55 $\mu\text{W}$

relative standard deviation for gain, 0.17% for gain-bandwidth-product, 2.45% for lower 3dB cut-off and 8.06% for upper 3dB cut-off. The monte carlo simulation results for individual runs could be seen in Figure 11 .

The common-mode rejection ratio (CMRR) and the power-supply rejection ratio (PSRR) were measured and both exceeded 80 dB. This is an important parameter for biomedical readout interfaces as our main objective is to reduce the common mode noise as much as possible and reject power supply variations and noise. A comparative analysis of this design with state-of-the-art designs is also given in Table 2 .

**FIGURE 11** Process Variation Analysis

## 5 | BIOLOGICAL DATA SIMULATION

We tested the circuit's performance using ECG waves with a maximum peak-to-peak voltage of 1.12 mV by using the suggested ECG Amplifier and a test signal from [T.S (2005)]<sup>16</sup> [Goldberger et al]<sup>17</sup>. Figure 12 shows the transient simulation of the

circuit, showing that it was able to amplify the wave up to 400 mV which is necessary for proper signal conversion by an analog to digital converter<sup>18</sup>. This amplifier can be deployed in pacemakers as a pre-amplifier before the peak detection stage<sup>19</sup>, due to its large bandpass response. The large bandpass response confirms the detection of all the QRS peaks at every cardiac cycle.

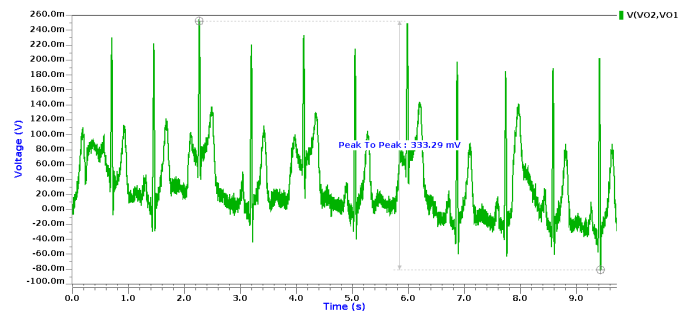


FIGURE 12 Biological Test Signal

## 6 | CONCLUSIONS

A 3 mHz to 880 Hz bandpass response with an input-referred noise of  $14.5 \mu V_{rms}$  across a  $2.55 \mu W$  fully integrated CMOS ECG amplifier has been demonstrated. The amplifier has no off-chip components and eliminates dc offsets that are frequently present in micro-electrode recording applications while passing low-frequency signals in the milli-hertz region. We were able to achieve the best power-noise trade-off among ECG amplifiers by taking advantage of the significant percentage of devices operating in weak inversion. Due to the elimination of even order harmonics, the fully differential design enables us to provide outputs with even low noise levels.

The number of channels will likewise rise in a comprehensive ECG recording system, and an ADC must be linked after the pre-amplifier. The ADC in such circumstances serves as a major source of power consumption. The pre-amplifier aids in boosting weak cardiac signals' millivolt voltage swing to a range that is suitable for optimal readability.

### 6.1 | Bibliography

#### References

1. Fay L, Misra V, Sarpeshkar R. A Micropower Electrocardiogram Amplifier. *IEEE Transactions on Biomedical Circuits and Systems* 2009; 3(5): 312-320. doi: 10.1109/TBCAS.2009.2026483
2. Malmivuo J, Plonsey R. *Bioelectromagnetism: Principles and Applications of Bioelectric and Biomagnetic Fields*. Oxford University Press . 1995
3. Sigma A. Silver Chloride Safety Datasheet.
4. Baba A, Burke MJ. Electrical Characterisation of Dry Electrodes for ECG Recording. In: ICC'08. World Scientific and Engineering Academy and Society (WSEAS); 2008; Stevens Point, Wisconsin, USA: 76–81.
5. Maji S, Burke MJ. The Skin-Electrode Interface Impedance and the Transient Performance of ECG Recording Amplifiers. In: ; 2018: 1-4
6. Winter BB, Webster JG. Driven-right-leg circuit design. *IEEE Transactions on Biomedical Engineering* 1983; BME-30(1): 62-66. doi: 10.1109/TBME.1983.325168
7. Harrison R, Charles C. A low-power low-noise CMOS amplifier for neural recording applications. *IEEE Journal of Solid-State Circuits* 2003; 38(6): 958-965. doi: 10.1109/JSSC.2003.811979

8. Tsitouras A, Plessas F, Birbas M, Kikidis J, Kalivas G. A sub-1V supply CMOS voltage reference generator. *International Journal of Circuit Theory and Applications* 2012; 40(8): 745-758. doi: <https://doi.org/10.1002/cta.753>
9. Young B. New standards for ECG equipment. *Journal of Electrocardiology* 2019. doi: 10.1016/j.jelectrocard.2019.07.013
10. Jespers PGA, Murmann B. *Systematic Design of Analog CMOS Circuits: Using Pre-Computed Lookup Tables*. Cambridge University Press . 2017
11. Najafi K, Wise K. Implantable multielectrode array with on-chip signal processing. In: . XXIX. ; 1986: 98-99
12. Berson AS, Pipberger HV. The low-frequency response of electrocardiographs, a frequent source of recording errors.. *American heart journal* 1966; 71 6: 779-89.
13. Guillory K, Normann R. A 100-channel system for real time detection and storage of extracellular spike waveforms. *Journal of Neuroscience Methods* 1999; 91(1): 21-29. doi: [https://doi.org/10.1016/S0165-0270\(99\)00076-X](https://doi.org/10.1016/S0165-0270(99)00076-X)
14. Zhang J, Zhang H, Sun Q, Zhang R. A Low-Noise, Low-Power Amplifier With Current-Reused OTA for ECG Recordings. *IEEE Transactions on Biomedical Circuits and Systems* 2018; 12(3): 700-708. doi: 10.1109/TBCAS.2018.2819207
15. Saeidian F, Ashraf M. An ultra-low-power, low-noise tunable electrocardiogram amplifier. *International Journal of Circuit Theory and Applications* 2020; 48(11): 1975-1989. doi: <https://doi.org/10.1002/cta.2867>
16. T.S L. Biometric human identification based on electrocardiogram. Master's thesis. 2005.
17. Goldberger AL, Amaral LAN, Glass L, et al. PhysioBank, PhysioToolkit, and PhysioNet: Components of a New Research Resource for Complex Physiologic Signals. *Circulation* 2000 (June 13); 101(23): e215–e220.
18. Duan Q, Jung Y, Choi D, Roh J, Kim J. A 1.2V 83dB DR single-ended input SC DS modulator including a large-swing analog buffer for portable ECG applications. *International Journal of Circuit Theory and Applications* 2016; 44(12): 2164-2173. doi: <https://doi.org/10.1002/cta.2219>
19. Kumar A, Komaragiri R, Kumar M. Design of efficient fractional operator for ECG signal detection in implantable cardiac pacemaker systems. *International Journal of Circuit Theory and Applications* 2019; 47(9): 1459-1476. doi: <https://doi.org/10.1002/cta.2667>
20. Sarpeshkar R. *Ultra Low Power Bioelectronics: Fundamentals, Biomedical Applications, and Bio-Inspired Systems*. Cambridge University Press . 2010
21. Maji S, Burke MJ. Establishing the Input Impedance Requirements of ECG Recording Amplifiers. *IEEE Transactions on Instrumentation and Measurement* 2020; 69(3): 825-835. doi: 10.1109/TIM.2019.2907038
22. Burke M, Gleeson D. A micropower dry-electrode ECG preamplifier. *IEEE Transactions on Biomedical Engineering* 2000; 47(2): 155-162. doi: 10.1109/10.821734
23. Gray PR, Meyer RG, Hurst PJ, Lewis SH. *Analysis and Design of Analog Integrated Circuits*. USA: John Wiley and Sons, Inc. 4th ed. 2001.
24. Stefanović D, Kayal M. *Structured Analog CMOS Design* . 2008
25. Johns D, Martin K. *Analog Integrated Circuit Design*. Wiley India Pvt. Limited . 2008.
26. Li M, Sun Y. General rational approximation of Gaussian wavelet series and continuous-time gm-C filter implementation. *International Journal of Circuit Theory and Applications* 2020; 48(11): 2006-2022. doi: <https://doi.org/10.1002/cta.2834>
27. Lee SY, Liang MC, Tsai TH, Kao WC. Analysis and implementation of a fourth-order bandpass filter for R-wave detection of an implantable cardiac microstimulator. *International Journal of Circuit Theory and Applications* 2013; 41(11): 1188-1202. doi: <https://doi.org/10.1002/cta.1828>

